IOPscience iopscience.iop.org

Home Search Collections Journals About Contact us My IOPscience

Confinement of excitons in spherical quantum dots

This article has been downloaded from IOPscience. Please scroll down to see the full text article.

1998 J. Phys.: Condens. Matter 10 1349

(http://iopscience.iop.org/0953-8984/10/6/017)

View the table of contents for this issue, or go to the journal homepage for more

Download details:
IP Address: 171.66.16.209
The article was downloaded on 14/05/2010 at 12:14

Please note that terms and conditions apply.

J. Phys.: Condens. Matter **10** (1998) 1349–1361. Printed in the UK PII: S0953-8984(98)85158-8

Confinement of excitons in spherical quantum dots

J L Marín†, R Riera‡ and S A Cruz§

† Centro de Investigación en Física, Universidad de Sonora, Apartado Postal 5-088, 83190, Hermosillo, Sonora, Mexico

‡ Departamento de Física de la Universidad de Sonora, Apartado Postal 1626, 83000 Hermosillo Sonora, Mexico

§ Departamento de Física, Universidad Autónoma Metropolitana–Iztapalapa, Apartado Postal 55-534, 09340, Mexico DF, Mexico

Received 11 June 1997, in final form 18 November 1997

Abstract. The ground-state energy of excitons confined in microspherical crystallites with a finite-height potential wall is studied variationally as a function of the particle radius in the so-called strong-confinement regime. Exciton energies for dot radii in the range 5–40 Å are calculated and compared with experimental and theoretical data for CdS, CdSe, PbS and CdTe crystallites. This comparison shows that the effective-mass approximation and spherical confinement geometries are appropriate for all of the particle sizes. Our results also show that the quantum dot cannot be modelled using an infinite-barrier-height potential in the strong-confinement regime.

1. Introduction

The study of quantum-size effects for semiconductor microcrystals has become a subject of interest due to the effect of confinement on Wannier excitonic state: it produces important changes in the optical properties of microcrystallites as compared to those of the corresponding bulk material (Brus 1986a, b, Wang and Herron 1991, Yamamoto *et al* 1991, Morgan *et al* 1990).

There have been several theoretical efforts to account for the size dependence of the energy levels of excitons confined by small spherical quantum dots (Brus 1983, Schmidt and Weller 1986, Weller *et al* 1986, Nair *et al* 1987, Wang *et al* 1987). There are two limiting cases, depending upon the ratio between the radius of the quantum dot r_0 and the effective Bohr radius of the bulk exciton a. For $r_0/a \gg 1$ the exciton can be envisioned as a quasiparticle moving around inside the quantum dot with only little energy increment due to confinement; in this case, the infinite-potential-well model (within the single-band effective-mass approximation (EMA)) gives a reasonable description of the experimentally observed shift in the exciton ground-state energy. The latter is also true for other treatments such as that based on the effective-bond-orbital model (EBOM) (Einevoll 1992), the tight-binding (TB) approach (Lippens and Lannoo 1989, 1990) and the semi-empirical pseudopotential method (SEPM) (Wang and Zunger 1996). In the opposite limit, $r_0/a \ll 1$, the confinement effect dominates and the electron and hole should be viewed as individual particles predominantly in their respective single-particle ground states with only little spatial correlation between them. In this regime (called the strong-confinement regime), the exciton in the quantum dot 'feels' the boundary effects strongly, and the inclusion of a finite height for the confining potential barrier has become an important requirement in

0953-8984/98/061349+13$19.50 © 1998 IOP Publishing Ltd

order to account for recent experiments on the optical properties of small crystallites (Wang and Herron 1991, 1990). This has been confirmed recently by our calculations and other work (Kayanuma 1990, Einevoll 1992).

The aim of this work is to show that a recently developed strategy using the direct variational method, which is remarkably simple and particularly useful for the treatment of confined quantum systems (Marín and Cruz 1992), provides reasonable answers in the study of real systems. To this end, we analyse the effect of confinement on the ground-state energy of an electron–hole pair trapped in a microspherical crystallite with finite-barrier potential walls by imposing appropriate boundary conditions. Our results are compared with those obtained from previous, more sophisticated theoretical calculations and recent experiments on CdTe, CdSe, PbS and CdS crystallites embedded in different host materials. A critical size of the crystallite below which the exciton deconfines is predicted, in contrast to the case for the above-mentioned theoretical approaches in which this limit does not exist.

The following assumptions are made in our treatment: (i) the EMA in the single-band scheme (parabolic with zero spin splitting) is valid for all particle sizes; (ii) surface and image potential effects can be neglected; (iii) the lattice reconstruction is different from that for the bulk material; and (iv) the quantum dots have an approximate spherical shape for all sizes, keeping the same dielectric constant as their corresponding bulk material.

Although the above hypotheses are known to be too crude for the smaller crystallite sizes (Brus 1986a, b, 1984), we believe that the physical information provided by this treatment should be independent of a more detailed account of the features mentioned above, being correct for real structures. Comparison of the results of this work with those of a set of recent experiments on CdS (Wang and Herron 1990), CdTe (Ramírez *et al* 1995), PbS (Wang and Herron 1991) and CdSe (Wang and Zunger 1996) crystallites embedded in different materials clearly points to the need to go beyond the EMA and spherical confinement to account for the exciton energies observed for the smallest particle sizes.

2. The model and applied theory

In the EMA, the model Hamiltonian for the system of interest is (taking $\hbar = e = 1$)

$$\hat{H} = -\frac{1}{2m_e}\nabla_e^2 - \frac{1}{2m_h}\nabla_h^2 - \frac{1}{\varepsilon|\boldsymbol{r}_e - \boldsymbol{r}_h|} + V_e + V_h \tag{1}$$

where ε stands for the dielectric constant, m_e (m_h) is the electron (hole) effective mass relative to the free-electron mass, $\boldsymbol{r}_e$ ($\boldsymbol{r}_h$) is the electron (hole) position relative to the centre of the sphere and V_e (V_h) is the barrier height of the confining potential for the electron (hole). Assuming the same barrier (V_0) for electrons and holes,

$$V_e = V_h = \begin{cases} 0 & 0 \leqslant r_e, r_h \leqslant r_0 \\ V_0 & r_0 \leqslant r_e, r_h < \infty \end{cases} \tag{2}$$

where r_0 is the radius of the sphere. Physically, V_0 in this context simulates the average effective potential step created by the difference in composition between the crystallite and the host material.

Note that the structure of (1) is similar to that for the helium atom except that the electron–electron repulsion term is replaced by the attractive electron–hole interaction and the nuclear charge term (Z) becomes zero in this case. Hence, in contrast with previous variational calculations related to this problem (Nair *et al* 1987, Kayanuma 1990, 1988), here the strategy used in the treatment of the confined helium atom is followed, i.e. the wavefunction *ansatz* for the exciton is constructed as a product of two 1s hydrogenic

functions, as was described previously (Marín and Cruz 1992). Accordingly, the ground-state wavefunction in the interior region ($0 \leqslant r_e, r_h \leqslant r_0$) is defined as

$$\psi_i = A \exp\left[-\alpha(r_e + r_h)\right](r_0 - \alpha r_h)(r_0 - \alpha r_h) \tag{3}$$

while for the exterior region ($r_0 \leqslant r_e, r_h < \infty$)

$$\psi_o = B(r_e r_h)^{-1} \exp\left[-\beta(r_e + r_h)\right] \tag{4}$$

where α and β are variational parameters to be determined after minimization of the total energy, with additional constraints, imposed by the following boundary condition:

$$\left.\frac{1}{m_i^*}\frac{1}{\psi_i}\frac{\partial \psi_i}{\partial r_s}\right|_{r_s=r_0} = \left.\frac{1}{m_o^*}\frac{1}{\psi_o}\frac{\partial \psi_o}{\partial r_s}\right|_{r_s=r_0} \tag{5}$$

where the subscript s is generic, standing for either electron or hole, and m_i^* and m_o^* correspond to the reduced effective mass of the exciton inside and outside the quantum dot (QD). In the above equation we have introduced a relation between the effective masses as a criterion for differentiating between the excitons in the two regions where, indeed, there are different materials (Trallero-Giner and Lopez-Gondar 1985). Note also that this boundary condition is not the same as the usual one in the sense that, in the latter, the electron is assumed to have the same mass in both regions (inside and outside the well), an assumption which does not strictly hold true in the present case. Furthermore, as the electron is deconfined before the hole, we can consider that, as a reasonable approximation, the variation of the exciton reduced mass is mainly due to the change in the electron effective mass, while the hole effective mass remains the same. Equation (5) connects α and β as follows:

$$\beta = \frac{q\left[\alpha r_0(1-\alpha) + \alpha\right] + \alpha - 1}{r_0(1-\alpha)} \tag{6}$$

with $q = m_o^*/m_i^*$.

Hence we only need to determine one of the variational parameters. The constants A and B can be determined through the normalization condition

$$\langle \psi_i | \psi_i \rangle + \langle \psi_o | \psi_o \rangle = 1 \tag{7}$$

and the continuity of the wavefunction $\psi_i = \psi_o$ at $r = r_0$.

The expectation value of $\hat{H}$ (or the corresponding energy functional E) can be constructed using equations (1)–(7) (see the appendix) and the parameter α (or β) can be found through the minimization of E in the standard fashion, i.e.

$$\frac{\partial E}{\partial \alpha} = 0 \qquad \text{or} \qquad \frac{\partial E}{\partial \beta} = 0. \tag{8}$$

In the present work the expression for the energy functional was found analytically and its minimization was carried out numerically with a precision of the order of 10^{-4}. As the reader must be aware, the procedure followed to perform the calculations is quite simple. Indeed, it takes only a few minutes to construct a given curve of the exciton ground-state energy as a function of the crystallite size.

3. Discussion of the results

Figure 1 shows the experimental values and theoretical predictions for the exciton ground-state energy in CdS crystallites of various sizes, embedded in an organic material (circles) (Wang and Herron 1990) as well as in silicate glass (triangles) (Ekimov *et al* 1985).

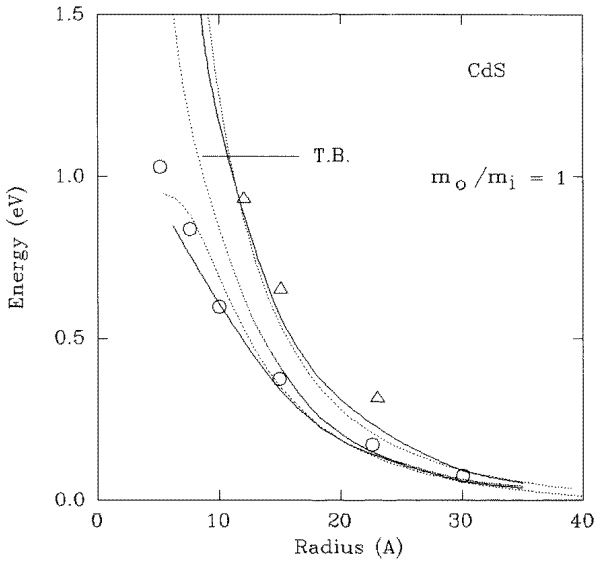

Figure 1. Energies for excitons in CdS crystallites as functions of their sizes. The symbols represent the experimental data for crystallites embedded in different materials: organic material (circles) and silicate glass (triangles). The continuous curves correspond to the EBOM calculations while the dashed ones correspond to the variational results of the present work. The curve labelled 'T.B.' corresponds to the results of the tight-binding calculations. The band gap for CdS has been subtracted from the confined exciton energy.

The solid lines represent the theoretical prediction made by Einevoll (1992) who carried out an analysis of exciton confinement in CdS quantum dots, based on the effective-bond-orbital model (EBOM) for the hole and the effective-mass approximation (EMA) for the electron with a finite-barrier-height potential. The higher curve corresponds to $V_e = V_h = V_0 = 2.25$ eV and the lower one to 0.50 eV. The dashed line, labelled 'T.B.', represents theoretical predictions made by Lippens and Lannoo (1989, 1990) who carried out an analysis of exciton confinement in CdS quantum dots based on the tight-binding method assuming an infinite-barrier-height potential model. The other dashed lines represent our theoretical prediction based on the effective-mass approximation model in the single-band scheme and the variational method. The higher curve corresponds to $V_0 = 2.50$ eV and $m_o/m_i = 1$ and the lower curve to 0.475 eV and $m_o/m_i = 1.0$. In all cases the results were evaluated for the same CdS material parameters (Lippens and Lannoo 1989, 1990) ($m_e = 0.18m_o$, $m_h = 0.53m_o$ and $\varepsilon = 5.5$, $m_o =$ free-electron mass) and the gap energy in the bulk material $E_g = 2.5$ eV (Lippens and Lannoo 1989, 1990) has been subtracted from the total exciton energy (E_{ex}); i.e. $E_0 = E_{ex} - E_g$. The analysis of this figure shows the following.

(i) The same quantum dots embedded in different materials show different experimental values of the exciton ground-state energy, demonstrating that the exciton energy in the quantum dot depends upon the exterior medium in which it is synthesized.

(ii) In the strong-confinement regime no model based on infinite-height potential barriers can give a reasonable description of the experimentally observed shift in the exciton ground-state energy as a function of the quantum dot size. This indicates that the assumption of a finite barrier height and the introduction of the effective mass in the boundary condition

would be essential to achieve a good agreement between theory and experiment.

(iii) Our EMA-based variational method gives similar results to the EBOM calculation which requires a more elaborate treatment. In addition, an important qualitative feature appears in the present calculations: a difference in the slope of the energy curve for small particle radius as compared with the EBOM calculation.

The onset for the vanishing of the well states is clearly present in the results of this work; that is, given a barrier height, there exists a critical particle radius (when $E_0 = V_e = V_h = V_0$) below which the exciton is no longer confined. The latter is more evident in the lower curve in figure 1 ($V_0 = 0.475$ eV). Physically, the slope of the curve should be related to the confining force. In this case, we observe a decrease in the slope at about $r_0 \leqslant 12$ Å, which could correspond to the particle radius for which the electron is first deconfined, while the hole (due to its larger mass) is still confined. For particle radius $r_0 \approx 6$ Å ($E_0 = 0.95$ eV), the slope becomes zero, indicating complete deconfinement of the exciton. The same can be said for the rest of the curves. We believe that this qualitative effect should be present in any calculation.

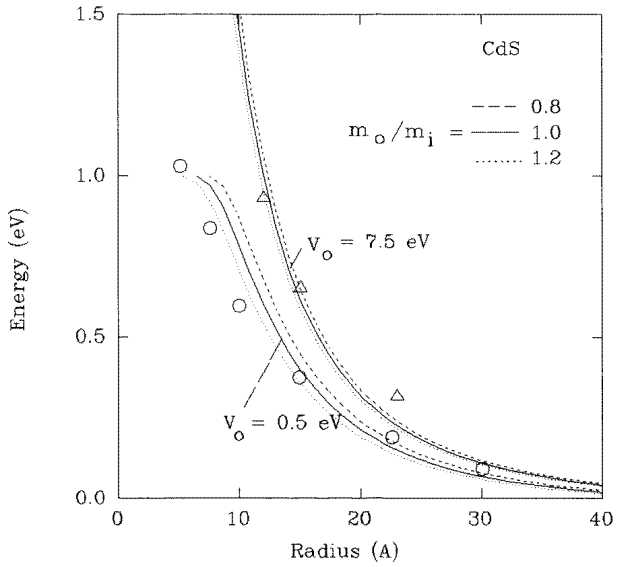

Figure 2. Energies for excitons in CdS crystallites as functions of their sizes. The symbols represent the experimental data for crystallites embedded in different materials: organic material (circles) and silicate glass (triangles). The curves correspond to the variational results of the present work, for different relations between the effective mass inside and outside the crystallite. The band gap for CdS has been subtracted from the confined exciton energy.

In figure 2 we compare the same experimental data for CdS as are presented in figure 1 with our theoretical results for two confining potentials of the electron and hole (which have been considered equal: $V_e = V_h = V_0$). We plot the exciton energy for $V_0 = 7.5$ eV (higher curves), $V_0 = 0.5$ eV (lower curves) and three different values of m_o/m_i (0.8, 1.0, 1.2) for each value of the confining potential (in the same order as is indicated in the figure). The experimental data (indicated as triangles) correspond to CdS crystallites in silicate glass (Ekimov *et al* 1985) which have a gap energy of 7 eV in the barrier, as has been roughly estimated for this material by Kayanuma (1990) and Einevoll (1992). The experimental data indicated as circles (Wang and Herron 1990) correspond to lower barrier heights of

CdS crystallites embedded in an organic material. Note however that, since the crystallites were fabricated by two different techniques, their spherical shapes and the values of V_0 and m_i can change due to the inhomogeneity of the media. On the other hand, note that the experimental data indicated as triangles in figures 1 and 2 are same, but the curves corresponding to two different finite barrier heights in our results give a good agreement between theory and experiment, which is due to the fact that the gap energy of the silicate glass is very large, but finite. This is not the case for the experimental data indicated as circles where the barrier height potential is smaller, and they are more sensitive to the value chosen for V_0, as is corroborated when we use $V_0 = 0.475$ (circles in figure 1) and $V_0 = 0.5$ (circles in figure 2).

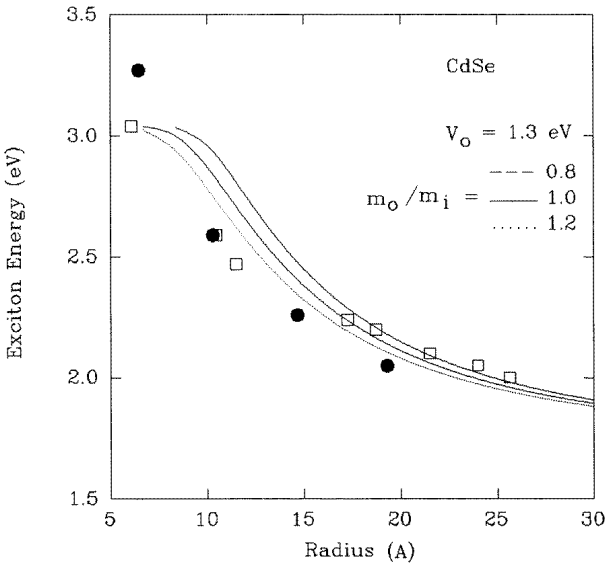

Figure 3. Energies for excitons in CdSe crystallites as functions of their sizes. Squares represent the experimental data while filled circles correspond to the pseudopotential calculation. The curves correspond to the variational results of the present work.

In figure 3 we show (filled circles) the theoretical predictions given by Wang and Zunger (1996) which are based on a plane-wave semi-empirical pseudopotential method (SEPM), with non-local potentials and spin–orbit coupling in a CdSe quantum dot. Wang and Zunger have also used a size-dependent dielectric constant in the Coulomb interaction energy. We also show (squares) the experimental data from Wang and Zunger (1996) and our theoretical results based on the EMA with the finite barrier height $V_0 = 1.3$ eV and different values of $m_o/m_i = 0.8$, 1.0 and 1.2. The calculations were performed with the parameters $m_e = 0.13m_o$, $m_h = 0.4m_o$, $\varepsilon = 10.6$. From this figure we can reach the following conclusions.

(i) Correction of the Coulomb interaction energy with a size-dependent dielectric constant is not sufficient to produce good agreement between experimental data and theoretical results for an exciton confined in the strong-confinement regime since the external medium in which the crystallite is embedded should be considered via a finite-height potential barrier and different effective masses (inside and outside the QD). The dielectric constant of the quantum dot $\varepsilon_{dot}(\infty)$ is only different from the bulk dielectric

constant $\varepsilon_{bulk}(\infty)$ for CdSe for $r_0 < 20$ Å, where decreases for small values of r_0 make the exciton energy smaller and the contribution (with a finite-height potential) is also too small to lead to a good agreement between the experimental data and the theoretical curve. The dielectric constant correction to the QD size with the infinite-potential model would not explain the experimental data in figure 1; for example, the TB calculation of Lippens and Lannoo (1989, 1990) with an infinite potential barrier only describes the experimental data represented by circles, but never the experimental data represented by triangles. Moreover, the theoretical curves based on infinite barriers always diverge when $r_0 \to 0$, but they converge when finite barriers are assumed.

(ii) The spin–orbit splitting in the valence-band structures is not very sensitive to the calculation of the ground-state energy of the exciton (see figure 5 of Lippens and Lannoo 1989, 1990).

(iii) The introduction of the effective mass in equation (5) would represent another variable which could take into account the exterior medium in which the crystallites are embedded.

(iv) If, in the effective-mass approximation with a finite-barrier-height potential, we include the size-dependent dielectric constant in the screening of the Coulomb interaction energy, we will obtain more accurate results for the exciton energy over this very small size range. Moreover, in the latter case, the theoretical curves would converge when $r_0 \to 0$.

Figure 4 shows the dependence of the optical band gap (the exciton energy) of PbS clusters (taken from Wang and Herron 1991) on the cluster size. The uppermost line represents an empirical EMA-based calculation (Wang and Herron 1991); this estimation contains only the basic physics of the quantum-size effects and it cannot be expected to be quantitatively correct in the strong-confinement regime, as has been shown by experimental

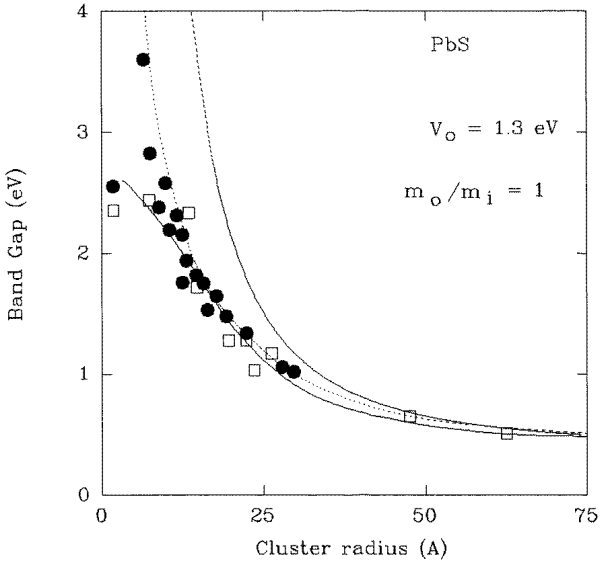

Figure 4. The band gap for a PbS cluster. The uppermost curve corresponds to the empirical EMA-based calculation, squares correspond to experimental data, filled circles correspond to the cluster tight-binding calculation, the dashed line corresponds to the hyperbolic band calculation and the solid curve represents the variational results of the present work.

studies and is indicated by its empirical character. Squares represent the experimental data, black circles represent the results of a cluster tight-binding calculation, the dashed curve represents the result of a hyperbolic band model calculation by Wang *et al* (1987) and the solid curve represents our results for $V_0 = 1.3$ eV and $m_o/m_i = 1$ (with $m_e = m_h = 0.1m_o$, $\varepsilon = 170$). As can be noticed, all of the theoretical methods based on the consideration of an infinite-barrier-height potential show a divergence with respect to the experimental data in the strong-confinement regime, but our results show a good agreement with the experimental data.

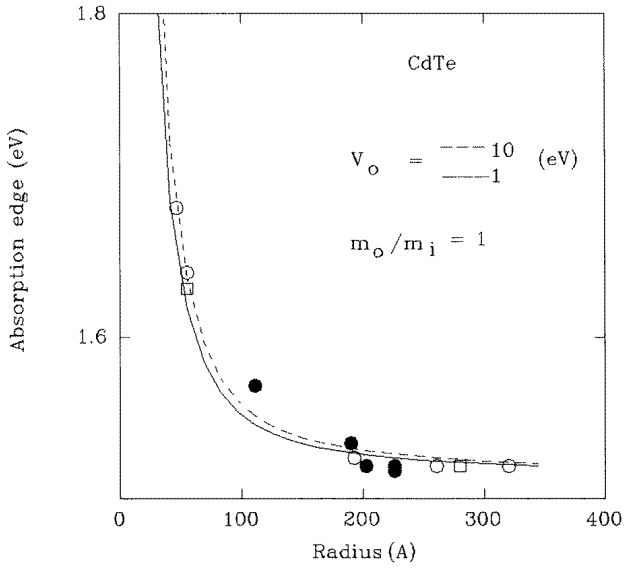

Figure 5. The absorption edge for a CdTe crystallite. Squares and circles (filled and hollow) represent the experimental data for crystallites prepared by the thermal annealing of CdTe:O with different oxygen concentrations. The curves correspond to the variational results of this work.

In figure 5 we show the experimental values for the absorption edge in CdTe crystallites of various sizes prepared by thermally annealing in an Ar flux the a-CdTe:O films deposited by rf sputtering obtained by Ramírez *et al* (1995). The different symbols correspond to three samples of a-CdTe:O annealed with different oxygen concentrations. The sizes of these quantum dots are in the weak-confinement regime; in this case, all of the methods based on infinite barriers potential give the same results. The dashed line corresponds to $V_0 = 10$ eV, which represents a big barrier potential, and the solid line corresponds to $V_0 = 1.0$ eV . The authors report a gap of 4.0 eV for $CdTeO_3$, obtaining an actual barrier potential of 1.25 eV per particle; as can be observed, there is only a small difference, which can be considered negligible for the two curves and the three samples. In this case the excitons do not 'feel' the boundary and the tunnelling probability is very small. For this material we have used $m_e = 0.11m_o$, $m_h = 0.35m_o$, $\varepsilon = 10.9$.

Finally, we have calculated the ground-state energy of an exciton confined in a spherical quantum dot using the effective-mass approximation with a finite-barrier-height potential in the single-band scheme as a function of the QD radius, applying the variational method, and we find a good agreement when we compare with different experimental data and other sophisticated theoretical methods which require more complex computational calculations.

We have also demonstrated that in the strong-confinement regime the QD cannot be modelled with an infinite-barrier potential, and that the introduction of the effective-mass relation between the electron and hole inside and outside of the QD allows a more accurate estimation of the ground-state exciton energy. Other models in which a finite barrier is not considered cannot explain the experimental data since the exciton energy $\to \infty$ as $r_0 \to 0$. Better theoretical results would be achieved if we incorporated a size-dependent dielectric constant and non-spherical confinement geometry. Further work is necessary to incorporate these features in the model in order to make final assessments of the usefulness and power of the simple variational approach used in this study.

Work is progress on this subject, and will be published in due course.

Acknowledgment

This work was supported in part by CONACYT (Mexico) under contract 4055-E.

Appendix. Construction of the energy functional

In the following we will describe, step by step, how one can construct the energy functional for an exciton which is confined within a spherical quantum dot in the framework of the effective-mass approximation and the variational method, as proposed in the present work.

A1. Normalization

The trial wavefunction, equations (3) and (4), can be normalized according to

$$\int_{\Omega_i} |\psi_i|^2 \, \mathrm{d}\tau_e \, \mathrm{d}\tau_h + \int_{\Omega_o} |\psi_o|^2 \, \mathrm{d}\tau_e \, \mathrm{d}\tau_h = 1 \tag{A1}$$

where Ω_i (Ω_o) is the volume inside (outside) the quantum dot and $\mathrm{d}\tau_e$ ($\mathrm{d}\tau_h$) is the corresponding volume element. The wavefunction, equations (3) and (4), can be rewritten as follows:

$$\psi_i = A\varphi_i(r_e)\chi_i(r_h) \qquad 0 \leqslant r_e, r_h \leqslant r_0 \tag{A2a}$$

and

$$\psi_o = A\varphi_o(r_e)\chi_o(r_h) \qquad r_0 \leqslant r_e, r_h < \infty \tag{A2b}$$

where φ_i (or χ_i) has the structure

$$\varphi_i(u) = \exp(-\alpha u)(r_0 - \alpha u)$$

and, correspondingly, φ_o (or χ_o) can be written as

$$\varphi_o(u) = \frac{\mathrm{e}^{-\beta u}}{u}.$$

The normalization condition given by equation (A1) can then be written as

$$A^2 \int |\varphi_i(r_e)|^2 |\chi_i(r_h)|^2 \, \mathrm{d}\tau_e \, \mathrm{d}\tau_h + B^2 \int |\varphi_o(r_e)|^2 |\chi_o(r_h)|^2 \, \mathrm{d}\tau_e \, \mathrm{d}\tau_h = 1 \tag{A3}$$

but

$$\int_{\Omega_i} |\varphi_i(r_e)|^2 \, \mathrm{d}\tau_e = \int_{\Omega_i} |\chi_i(r_h)|^2 \, \mathrm{d}\tau_h$$

and

$$\int_{\Omega_o} |\varphi_o(r_e)|^2 \, \mathrm{d}\tau_e + \int_{\Omega_o} |\chi_o(r_h)|^2 \, \mathrm{d}\tau_h.$$

Since the kernel functions in the integrals have the same structure, we have that

$$A^2 I_{N_i}^2 + B^2 I_{N_o}^2 = 1$$

with

$$I_{N_i} \equiv \int_{\Omega_i} |\varphi_i(r_e)|^2 \, \mathrm{d}\tau_e = \int_{\Omega_i} |\chi_i(r_h)|^2 \, \mathrm{d}\tau_h \equiv 2\pi \int_0^{r_0} \mathrm{e}^{-2\alpha u}(r_0 - \alpha u)^2 u^2 \, \mathrm{d}u \tag{A4}$$

and

$$I_{N_o} \equiv \int_{\Omega_o} |\varphi_o(r_e)|^2 \, \mathrm{d}\tau_e = \int_{\Omega_o} |\chi_o(r_h)|^2 \, \mathrm{d}\tau_h \equiv 2\pi \int_0^{r_0} \mathrm{e}^{-2\beta u} \, \mathrm{d}u = \frac{\pi}{\beta} \mathrm{e}^{-2\beta r_0}. \tag{A5}$$

Moreover, the continuity of the wavefunction at $r_e, r_h = r_0$ leads to

$$A\mathrm{e}^{-2\alpha r_0} r_0^2 (1-\alpha)^2 = B \frac{\mathrm{e}^{-2\beta r_0}}{r_0^2}$$

or

$$B = A\mathrm{e}^{-(2\alpha - 2\beta) r_0} r_0^4 (1-\alpha)^2.$$

The latter allows us to write the normalization constant A as

$$A = \left[I_{N_i}^2 + I_{N_o}^2 f \right]^{-1/2} \tag{A6}$$

where

$$f \equiv \mathrm{e}^{-(4\alpha - 4\beta) r_0} r_0^8 (1-\alpha)^4.$$

A2. Kinetic energy

The form of the wavefunction as given in equations (A2) allows us to write

$$\nabla_e^2 \psi_i = A \chi_i(r_h) \nabla_e^2 \varphi_i(r_e)$$
$$\nabla_h^2 \psi_i = A \varphi_i(r_e) \nabla_h^2 \chi_i(r_h).$$

Then the kinetic energy for the exciton inside the quantum dot is given as

$$\bar{K}_i = -\frac{1}{2m_e} \int_{\Omega_i} \psi_i^* \nabla_e^2 \psi_i \, \mathrm{d}\tau_e \, \mathrm{d}\tau_h - \frac{1}{2m_h} \int_{\Omega_i} \psi_i^* \nabla_h^2 \psi_i \, \mathrm{d}\tau_e \, \mathrm{d}\tau_h$$

or

$$\bar{K}_i = -\frac{A^2}{2me} \int_{\Omega_i} |\chi_i(r_h)|^2 \, \mathrm{d}\tau_h \int_{\Omega_i} \varphi_i^*(r_e) \nabla_e^2 \varphi_i(r_e) \, \mathrm{d}\tau_e - \frac{A^2}{2m_h} \int_{\Omega_i} |\varphi_i(r_e)|^2 \, \mathrm{d}\tau_e \int_{\Omega_i} \chi_i^*(r_h) \nabla_h^2 \chi_i(r_h) \, \mathrm{d}\tau_h$$

but, as we have pointed out before,

$$\int_{\Omega_i} |\varphi_i(r_e)|^2 \, \mathrm{d}\tau_e = \int_{\Omega_i} |\chi_i(r_h)|^2 \, \mathrm{d}\tau_h = I_{N_i}$$

and hence

$$\bar{K}_i = -\frac{A^2}{2m_e} I_{N_i} I_{k_i} - \frac{A^2}{2m_h} I_{N_i} I_{k_i} = -\frac{A^2}{2\mu} I_{N_i} I_{k_i} \tag{A7}$$

where

$$\frac{1}{\mu} = \frac{1}{m_e} + \frac{1}{m_h}$$

and μ is the reduced mass of the exciton and

$$I_{k_i} \equiv 2\pi \int_0^{r_0} \mathrm{e}^{-\alpha u}(r_0 - \alpha u)\left\{\left(\frac{\mathrm{d}^2}{\mathrm{d}u^2} + \frac{2}{u}\frac{\mathrm{d}}{\mathrm{d}u}\right)\mathrm{e}^{-\alpha u}(r_0 - \alpha u)\right\} u^2 \,\mathrm{d}u.$$

Accordingly, the kinetic energy for the exciton outside is given as

$$\bar{K}_o = -\frac{B^2}{2\mu} I_{N_o} I_{k_o} = -\frac{A^2 f}{2\mu} I_{N_o} I_{k_o}$$

where I_{N_o}, f were defined earlier and

$$I_{k_o} \equiv 2\pi \int_{r_o}^{\infty} \frac{\mathrm{e}^{-\beta u}}{u}\left\{\left(\frac{\mathrm{d}^2}{\mathrm{d}u^2} + \frac{2}{u}\frac{\mathrm{d}}{\mathrm{d}u}\right)\frac{\mathrm{e}^{-\beta u}}{u}\right\} u^2 \,\mathrm{d}u.$$

A3. Potential energy

The expectation value of $V_c = V_e + V_h$ can be written as

$$\bar{V}_c = \int_{\Omega_o} \psi_o^* V_c \psi_e \,\mathrm{d}\tau_e \,\mathrm{d}\tau_h = \int_{\Omega_o} \psi_o^* (V_e + V_h)\psi_o \,\mathrm{d}\tau_e \,\mathrm{d}\tau_h$$
$$= (V_e + V_h)B^2 \int_{\Omega_o} |\varphi_o(r_e)|^2 \,\mathrm{d}\tau_e \int_{\Omega_o} |\chi_o(r_h)|^2 \,\mathrm{d}\tau_h$$

or

$$\bar{V}_c = (V_e + V_h)B^2 I_{N_o}^2 = (V_e + V_h)A^2 f I_{N_o}^2.$$

The term for the electron–hole interaction can be expanded in spherical harmonics as

$$\frac{1}{|\boldsymbol{r}_e - \boldsymbol{r}_h|} = 4\pi \sum_{l=0}^{\infty} \sum_{m=-l}^{l} \frac{1}{(2l+1)} \frac{r_<^l}{r_>^{l+1}} Y_l^{m^*}(\theta_e, \phi_e) Y_l^m(\theta_h, \phi_h)$$

where $r_<$ ($r_>$) is the smaller (greater) of r_e and r_h.

With this expansion, the expectation value for the electron–hole interaction can be written as

$$\bar{V}_{eh} = -\int_{\Omega_i} \psi_i^* \frac{1}{|\boldsymbol{r}_e - \boldsymbol{r}_h|} \psi_i \,\mathrm{d}\tau_e \,\mathrm{d}\tau_h$$
$$= 4\pi A^2 \sum_{l=0}^{\infty} \sum_{m=-l}^{l} \frac{1}{(2l+1)} \int_{\Omega_i} \frac{r_<^l}{r_>^{l+1}} |\varphi_i(r_e)|^2 |\psi_i(r_h)|^2$$
$$\times\ Y_l^{m^*}(\theta_e, \phi_e) Y_l^m(\theta_h, \phi_h) r_e^2 r_h^2 \,\mathrm{d}\Omega_e \,\mathrm{d}\Omega_h \,\mathrm{d}r_e \,\mathrm{d}r_h$$

where $\mathrm{d}\Omega_e$ ($\mathrm{d}\Omega_h$) denotes the solid angle for the electron (hole).

As φ_i (or χ_i) does not depend on the angles (θ_e, ϕ_e) (or (θ_h, ϕ_h)),

$$\int Y_l^{m^*}(\theta_e, \phi_e) \,\mathrm{d}\Omega_e = \sqrt{4\pi} \int Y_l^{m^*}(\theta_e, \phi_e) Y_0^0(\theta_e, \phi_e) \,\mathrm{d}\Omega_e = \sqrt{4\pi}\delta_{l0}\delta_{m0}$$

and

$$\int Y_l^{m^*}(\theta_h, \phi_h) \,\mathrm{d}\Omega_h = \sqrt{4\pi} \int Y_0^{0^*}(\theta_h, \phi_h) Y_l^m(\theta_h, \phi_h) \,\mathrm{d}\Omega_h = \sqrt{4\pi}\delta_{l0}\delta_{m0}.$$

Thus,

$$\bar{V}_{eh} = -4\pi A^2 \int_{\Omega_i} \frac{r_<^l}{r_>^{l+1}} \mathrm{e}^{-2\alpha r_e} \mathrm{e}^{-2\alpha r_h} (r_0 - \alpha r_e)^2 (r_0 - \alpha r_h)^2 r_e^2 r_h^2 \, \mathrm{d}r_e \, \mathrm{d}r_h$$

and the singularity at $r_e = r_h$ can then be removed in the usual way, leading to (for instance, if we integrate r_h from 0 to r_e ($r_> = r_e$ and $r_< = r_h$) and then from r_e to r_0 ($r_> = r_h$ and $r_< = r_e$))

$$\bar{V}_{eh} = -(4\pi)^2 A^2 \left\{ \int_0^{r_0} \mathrm{e}^{-2\alpha r_e} \{F(\alpha, r_e) + G(\alpha, r_e, r_0)\} \right\} r_e^2 \, \mathrm{d}r_e$$

with

$$F(\alpha, r_e) \equiv \frac{1}{r_e} \int_0^{r_e} \mathrm{e}^{-2\alpha r_h} (r_0 - \alpha r_h)^2 r_h^3 \, \mathrm{d}r_h$$

$$G(\alpha, r_e, r_0) \equiv r_e \int_{r_e}^{r_0} \mathrm{e}^{-2\alpha r_h} (r_0 - \alpha r_h)^2 r_h \, \mathrm{d}r_h$$

or, in a more compact notation,

$$\bar{V}_{eh} = -(4\pi)^2 A^2 J(\alpha, r_0)$$

where

$$J(\alpha, r_0) \equiv \int_0^{r_0} \mathrm{e}^{-2\alpha r_e} (r_0 - \alpha r_e)^2 \{F(\alpha, r_e) + G(\alpha, r_e, r_0)\} r_e^2 \, \mathrm{d}r_e.$$

A4. The energy functional

With the results of sections A1–A3, the energy functional $E(\alpha, r_0)$ can be constructed as

$$E(\alpha, r_0) = \bar{K}_i + \bar{K}_o + \bar{V}_{eh} + \bar{V}_c$$

in which the parameter β can be replaced by its corresponding value in terms of the parameters α and r_0 (equation (6)).

Finally, as the reader must be aware, the integrals involved in the construction of $E(\alpha, r_0)$ can be reduced to the form of incomplete Gamma functions, i.e. integrals of the form

$$\gamma(n, u) = \frac{1}{\Gamma(n)} \int_0^u \mathrm{e}^{-t} t^{n-1} \, \mathrm{d}t$$

or

$$\Gamma(n, u) = \Gamma(n) - \gamma(n, u) = \int_u^\infty \mathrm{e}^{-t} t^{n-1} \, \mathrm{d}t$$

which are well known and can be easily found in any table of integrals (see, for instance, Gradshteyn and Ryzhik 1980).

References

Brus L E 1983 *J. Chem.* **79** 5566
——1984 *J. Chem.* **80** 4403
——1986a *J. Chem.* **90** 2555
——1986b *IEEE J. Quantum Electron.* **22** 1909
Einevoll G T 1992 *Phys. Rev.* B **45** 3410
Ekimov A I, Efros A I L and Onushchenko A A 1985 *Solid State Commun.* **56** 921
Gradshteyn I M and Ryzhik I S 1980 *Tables of Integrals, Series and Products* (San Diego, CA: Academic) p 310

Kayanuma Y 1988 *Phys. Rev.* B **38** 9797
——1990 *Phys. Rev.* B **41** 10 261
Lippens P E and Lannoo M 1989 *Phys. Rev.* B **39** 10 935
——1990 *Phys. Rev.* B **41** 6079
Marín J L and Cruz S A 1991 *J. Phys. B: At. Mol. Opt. Phys.* **24** 2899
——1992 *J. Phys. B: At. Mol. Opt. Phys.* **25** 4365
Morgan R A, Park S H, Koch S W and Peyghambarian N 1990 *Semicond. Sci. Technol.* **5** 544
Nair S V, Sinha S and Rustagi K C 1987 *Phys. Rev.* B **35** 4098
Ramírez R, Espinoza F J, Arispe H, Zelaya O and Sanchez F 1995 *J. Appl. Phys.* **77** 5461
Schmidt H M and Weller H 1986 *Chem. Phys. Lett.* **129** 615
Trallero-Giner C and Lopez-Gondar J 1985 *Physica* B **138** 287
Wang W L and Zunger A 1996 *Phys. Rev.* B **53** 9579
Wang Y and Herron N 1990 *Phys. Rev.* B **42** 7253
——1991 *J. Phys. Chem.* **95** 525
Wang Y, Suna A, Mahler W and Kasowki R 1987 *J. Chem. Phys.* **87** 7315
Weller H, Schmidt H M, Koch U, Fojtik A, Baral S, Henglein A, Kunath W, Weiss K and Diemann E 1986 *Chem. Phys. Lett.* **124** 557
Yamamoto M, Hayashi R, Tsunemoto K, Kohno K and Osaka Y 1991 *Japan. J. Appl. Phys.* **30** 136